Direct Measurement of the Friction between and Shear Moduli of Shells of Carbon Nanotubes

Letian Lin,[1] Taoran Cui,[2] Lu-Chang Qin,[1,2] and Sean Washburn[1,2,3,4]

[1]*Curriculum in Applied Sciences and Engineering, University of North Carolina at Chapel Hill, Chapel Hill, North Carolina 27599-3255, USA*

[2]*Department of Physics and Astronomy, University of North Carolina at Chapel Hill, Chapel Hill, North Carolina 27599-3255, USA*

[3]*Department of Computer Science, University of North Carolina at Chapel Hill, Chapel Hill, North Carolina 27599-3255, USA*

[4]*Department of Biomedical Engineering, University of North Carolina at Chapel Hill, Chapel Hill, North Carolina 27599-3255, USA*

(Received 26 May 2011; published 7 November 2011)

We report measurements of the shear modulus of each shell and the friction between the two shells of double-shell carbon nanotubes in single nanotube-based nanoelectromechanical devices operated in a transmission electron microscope. *In situ* nanobeam electron diffraction is applied to obtain the chiral indices of each shell of the nanotube and it allows us to establish a quantitative correlation between the atomic structure and properties of the nanotube under investigation.

DOI: 10.1103/PhysRevLett.107.206101 PACS numbers: 68.65.−k, 81.07.−b

Friction is still poorly understood at the microscopic level. Since friction is the dominant force at small lengths in nanoelectromechanical structures, it is critical to obtain a detailed characterization for both fundamental understanding and potential applications of optimized nanoelectromechanical systems (NEMS). Carbon nanotubes (CNTs) [1–3] have attracted considerable research interest into their structure, physical properties, and applications in NEMS [4–8]. Nanoelectromechanical devices that depend on a single carbon nanotube, single-walled or multiwalled, as a torsional bearing, such as resonators, electronic motors, and switches, have been fabricated to study the torsional properties and interlayer interactions [9–14]. These manipulations and measurements, however, were done through the outermost shell of a multiwall carbon nanotube (MWNT) and no direct measurements or observations on the inner shell's response were possible in those experiments [11,13,15]. It is the purpose of this work to clarify the details of friction between the shells as well as to measure the shear modulus and structural deformation of each shell when a double-wall carbon nanotube (DWNT) is in torsional strain. In addition, nanobeam electron diffraction (NBED) is employed to obtain the exact chirality (chiral indices) and to reveal the atomic-scale deformation of each shell of the nanotubes [8]. Low-friction motion of the outer shells relative to the inner shells has been reported to occur (through a self-selecting process between the shells which have the least surface resistance) in a telescoping motion [16,17]. Here we present a direct measurement of the torsional motion of both shells of a DWNT under an external torque on the outer shell of the DWNT (see Fig. 1). The shear modulus of each shell and the interlayer friction are inferred from direct measurements of each shell's deformation, van der Waals interactions between shells, and reliable models of lattice strain.

Individual DWNTs were grown on a 50 μm thick silicon membrane with a 300 nm Si_3N_4 layer and a 200 nm SiO_2 layer. Metal anchors, a side electrode (''gate''), and a paddle, consisting of a 3 nm Cr adhesion layer and 60 nm Au layer, were patterned onto a DWNT by electron beam lithography and thermal evaporation. HNA (HF, HNO_3, and CH_3COOH) was used to remove 50 μm of Si from the back side of the wafer beneath the device. Focused ion beam (FIB) was used to etch three windows (1.5 μm $\times$ 1.8 μm) in the Si_3N_4 membrane below the 3 CNT segments among the 4 metal anchors. Buffered HF was then used to etch the 200 nm SiO_2 layer beneath the device followed by a critical point drying, leaving three freely-suspended segments of the same DWNT—one with the paddle, as schematically shown in Fig. 1.

The paddle actuation is performed *in situ* in a transmission electron microscope (TEM) via a voltage between

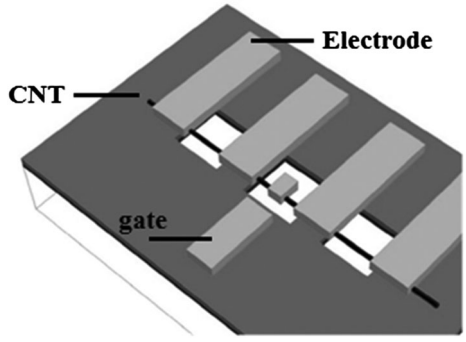

FIG. 1. Schematic of the device which is ready for electrical actuation and *in situ* electron diffraction analysis in TEM. The exposed parts of the nanotube are used for acquiring TEM images and electron diffraction patterns.

the paddle and the gate. The TEM allows NBED patterns of the DWNT before and while it is strained, and permits us to determine the chiral indices of both shells and the deformation of the shell lattices under strain. TEM images and NBED patterns are acquired at beam energy of 120 keV with a total electron irradiation dosage of about 10^{19} electrons/cm^2. Although knock-on damage is possible at these energies, we observed none.

Figure 2(a) is a TEM image of the CNT in the device which shows clearly that it is a DWNT. TEM images of the paddle as it is actuated are given in Figs. 2(b)–2(d). They show deflections of 90°, 117°, and 147° under dc biases of 0, 40, and 60 V applied to the gate. Once the dc bias was removed, the paddle returned to its initial state suggesting that the applied electrostatic torque accounts for all of the observed strain. The angular deflection of the paddle and hence the net strain in the outer shell are measured directly from changes in the projected length of the paddle. For each of these paddle positions, NBED patterns, Figs. 2(f)–2(h), were recorded from segments on the right or left side of the paddle. To determine the chiral indces of the unstrained CNT, NBED patterns on the segments between the other anchors were taken. From the NBED pattern [Fig. 2(e)] and the diameter measured in direct image mode, the chiral indice (u, v) of the DWNT were identified as (56,2) (37,18) from $v/u = (2D_2 - D_1)/(2D_1 - D_2)$, where D_1, D_2 and D_3 are the layer line spacings relative to the equatorial line for the principal layer lines L_1, L_2, and L_3, which are formed by Bragg reflections of graphene with Miller indices (10), $(\bar{1}0)$, and (11), respectively [18]. Layer lines L_4, L_5, L_6 are due to higher order Bragg reflections of graphene. NBED patterns were also recorded for each strain angle. Upon removal of the dc bias, the paddle returns to its initial position, indicating that the deformation is elastic.

CNTs are enantiomeric. When the nanotube is uniformly twisted along its axis, the pitch of the helix will be smaller or larger depending on the handedness of the nanotube relative to the sense of the twist. From measurement of D_1/D_2 under strain, we are able to calculate the twist angle of each shell by $\Delta\theta = [(2u + v)/(u + 2v) - D_1/D_2]/[D_1/D_2 - v/u]$ [19]. The uncertainty of the twist angle is $\pm 0.02°/\text{nm}$, and comes from two parts: (i) the resolution limit of diffraction pattern images (1 pixel out of 1024×1024 pixel image); (ii) the thermal excitations. Since the thermal oscillation is very small, we may assume that the inner shell had no strain and that the strain was only in the outermost shell [6]. With the device geometry and the tube diameter, $d = 4.45$ nm, we estimate that the thermal oscillation amplitude is no more than 2°, i.e., $0.003°/\text{nm}$.

The handedness of a carbon nanotube can be derived from diffraction patterns when it is twisted about its axis [19]. The layer line ratio D_1/D_2 will decrease for a right-handed nanotube and the ratio will increase for a left-handed one. We determined that the two shells of the

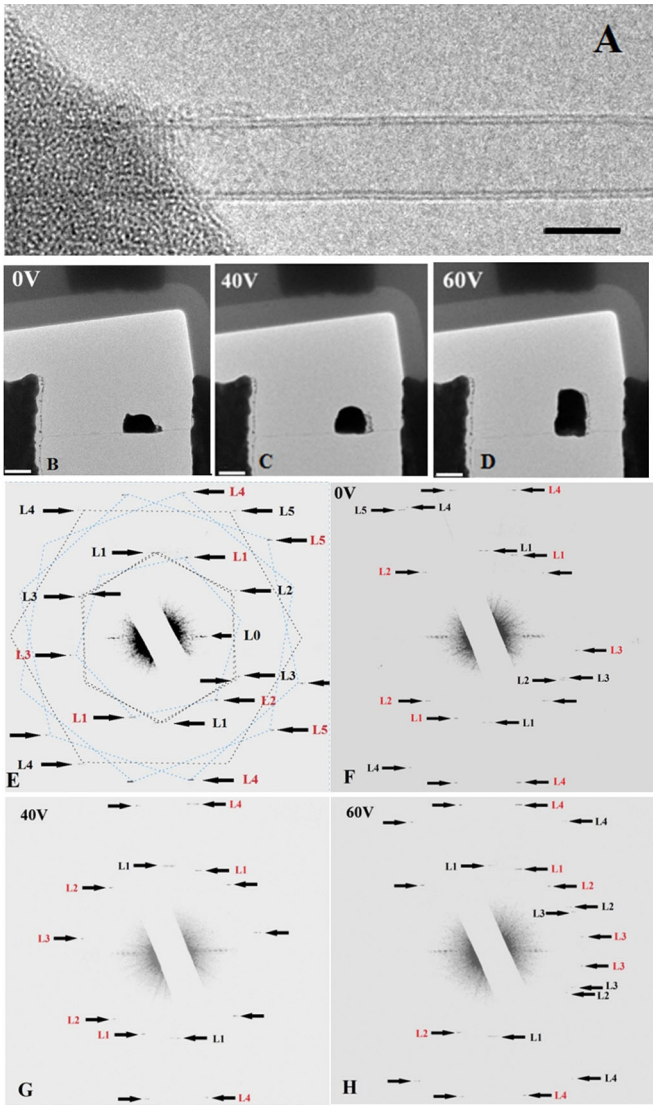

FIG. 2 (color online). TEM images and electron diffraction patterns of the suspended DWNT. The diffraction patterns are false-colored and marked by arrows. (A) High resolution TEM image of a typical DWNT employed in our devices. Scale bar, 5 nm. (B–D) TEM images of paddled device as it is actuated. They show deflections of 90°, 117°, and 147° under dc biases 0, 40, and 60 V applied to the gate. Scale bars, 200 nm. (E) Electron diffraction pattern of the DWNT taken from untwisted segment. The black letters and red letters indicate the diffraction layer lines of the outer shell and the inner shell, respectively. The two hexagons in black represent the primary reflections of graphene (10), $(\bar{1}0)$ and (11) from the outer shell and they form three principal layer lines L_1, L_2, and L_3 above and below the equatorial line, L_0. D_1, D_2, and D_3 are their respective layer line spacings measured from the equatorial line. The larger hexagons indicate the higher order reflections of graphene from the respective shells. The chiral indices of both shells, (56,2) (outer shell: diameter $d_o = 4.467$ nm, helicity $\alpha_o = 1.74°$) and (37,18) (inner shell: diameter $d_i = 3.805$ nm, helicity $\alpha_i = 18.72°$), are obtained from the diffraction data. (F–H) Electron diffraction patterns of the DWNT when the paddle is twisted under bias voltages of 0, 40, and 60 V. The deflection angles of the nanotube under torsion can be obtained from the shifts the diffraction layer lines.

TABLE I. Summary of the electron diffraction analysis of the DWNTs. Location indicates whether the nanotube diffraction pattern is taken at the right side or left side of the paddle. D_1/D_2 is the ratio of diffraction layer line spacings and $\Delta(D_1/D_2)$ gives the shift of diffraction layer lines when the nanotube is twisted: positive sign indicates that the layer lines move toward each other and negative sign indicates that the lines move away from each other. L is the length of the nanotube from the paddle to the anchor. $\Delta\theta$ and $\Delta\theta_{\mathrm{TEM}}$ are the twist angle along the tube calculated from the diffraction patterns and the rotation angle of the paddle measured in the TEM images.

Device	Gate Voltage (V)	Location	Shell	Handedness	D_1/D_2	$\Delta(D_1/D_2)$	L (nm)	Twisting Direction	$\Delta\theta(^\circ)$	$\Delta\theta_{\mathrm{TEM}}(^\circ)$	$\Delta\theta/L$ ($\pm 0.02^\circ$/nm)
1	0	Left	Outer	Right-Handed	1.950	−0.050	600	Counter clockwise	96 ± 12	90	0.16
			Inner		1.263	−0.003	600		6 ± 12		0.01
	40	Right	Outer		n/a	n/a	200	Clockwise	n/a	117	n/a
			Inner		1.241	0.019	200		14 ± 4		0.07
	60	Left	Outer		1.981	−0.081	600	Counter clockwise	150 ± 12	147	0.25
			Inner		1.272	−0.012	600		24 ± 12		0.04
	60	Right	Outer		1.698	0.202	200	Clockwise	146 ± 4	147	0.73
			Inner		1.236	0.024	200		18 ± 4		0.09
2	0	Left	Outer	Left-Handed	1.758	0.042	560	Counter clockwise	78.5 ± 11.2	66	0.14
			Inner		1.214	0.003	560		11.2 ± 11.2		0.02
	0	Right	Outer		1.926	−0.126	190	Clockwise	76 ± 3.8	66	0.4
			Inner		1.243	−0.026	190		15.2 ± 3.8		0.08
	15	Left	Outer		1.78	0.020	560	Counter clockwise	39.2 ± 11.2	55	0.07
			Inner		1.215	0.002	560		5.6 ± 11.2		0.01
	35	Left	Outer		1.791	0.009	560	Counter clockwise	16.8 ± 11.2	n/a	0.03
			Inner		1.221	−0.004	560		0 ± 11.2		0

DWNT (56, 2) (37, 18) in device 1 are both right-handed and the two shells of the DWNT (5, 65) (24, 44) in device 2 are both left handed.

Table I summarizes the results from our experiments on the two devices. Within its uncertainty, the twist of the outer shell matches the rotation angles of the paddle in device 1. This good match proves that the outer shell's stain is uniform because the diffraction patterns were taken at different parts of the CNT. More importantly, it assures that the measurements on the torsional movement of the inner shell by diffraction patterns are reliable (Therefore, we can use the paddle deflection angle from diffraction patterns, 117° measured from the paddle deflection to replace the undetermined outer shell twist at 40 V). We notice that the calculated twist angles of the outer shell are a bit off the paddle rotation angles in device 2, which might have been caused by vibrations or charging.

Figure 3 compares the strains of the inner shell to the outer shell. In contrast to the outer shell MWNT torsional model (where only outer shell twisted under an external torque) or the solid MWNT model (where all the shells twisted as a solid cylinder) [9], the inner shell actually strains in proportion to the outer shell but by a smaller amount (20% or less). The intercept indicates that the inner shell twisted with the outer shell with no stiction. It should also be noted that the intershell spacing for device 2 (0.310 nm) is smaller than that for device 1 (0.331 nm) and this is suggested to contribute to the slightly weaker torsional response of the inner shell in device 1 relative to the outer shell as indicated in Fig. 3. (We found intershell separations ranging from 0.31 to 0.35 nm in our ensemble of devices.)

Detailed knowledge of the device conformation, paddle geometry, shell strain, and dc bias voltages permit us to build an accurate finite element model to calculate the

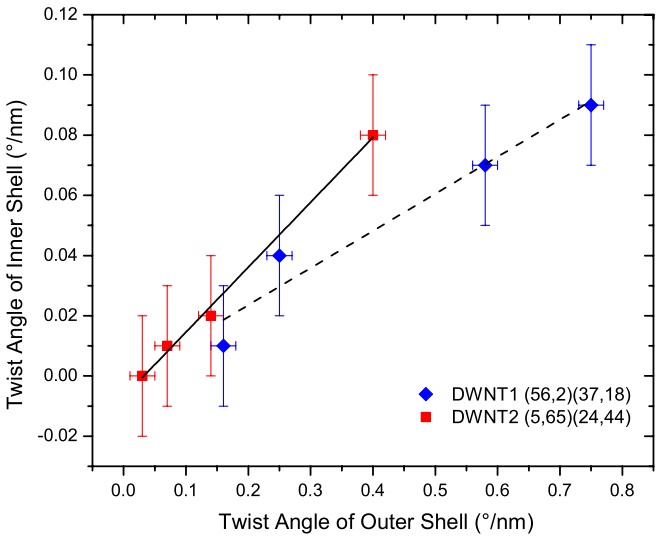

FIG. 3 (color online). The inner shell's torsional response to the twist of the outer shell of the two DWNT devices measured in this work. (■) DWNT1: (diameter $d_o = 4.467$ nm, helicity $\alpha_o = 1.74°$), ($d_i = 3.805$ nm, $\alpha_i = 18.72°$); (◆) DWNT2: ($d_o = 5.299$ nm, $\alpha_o = 3.67°$), ($d_i = 4.679$ nm, $\alpha_i = 20.36°$). The horizontal axis is the twist angle (°/nm) of outer shell and vertical axis (°/nm) is the twist angle of the inner shell.

external torque on the metal paddle [20]. The total electrostatic torque $\vec{\tau}$ on the paddle is given by the surface integral $\vec{\tau} = \frac{1}{\varepsilon_0} \iint_{\text{surface}} \sigma^2 \vec{R} \times \vec{n} dA$, where ε_0 is the vacuum permittivity, σ is the surface charge which is determined self-consistently, $\vec{n}$ is the local unit vector perpendicular to the paddle surface, dA is the infinitesimal surface area on the paddle, and $\vec{R}$ is the positional vector of dA from the DWNT axis. For each shell of the DWNT, the shear modulus G and torques τ_i applied on the nanotube are related by $G = \sum_i \tau_i l_1 l_2 / 2\pi r^3 \theta t (l_1 + l_2)$, where τ_i is the i-th torque applied on the shell, r is the radius of the concerned shell, $t = 0.34$ nm is the shell thickness, θ is the twist angle, and l_1, l_2 are the nanotube lengths to the left and right of the paddle [21]. The moduli of the outer and inner shells are 0.50 ± 0.01 T Pa and 0.41 ± 0.05 T Pa, respectively, in agreement with predictions [5]. The interlayer torque on the inner (or outer) shell, $\tau = r f_s$, where f_s is the static friction, at 40 and 60 V are $\tau_{40\ \text{V}} = (5.5 \pm 4.0) \times 10^{-18}$ N $\cdot$ M and $\tau_{60\ \text{V}} = (8.9 \pm 5.0) \times 10^{-18}$ N $\cdot$ M, respectively. If we assume that the interaction is uniform along the nanotube, the interlayer force, i.e., the static friction between the inner and outer shells at 40 and 60 V are then $f_{s,40\ \text{V}} = (2.7 \pm 1.9) \times 10^{-9}$ N, $[(3.4 \pm 2.2) \times 10^{-15}$ N/atom] and $f_{s,60\ \text{V}} = (4.3 \pm 2.4) \times 10^{-9}$N, $[(5.3 \pm 2.9) \times 10^{-15}$ N/atom], respectively. The difference between the static friction forces is due to the different van der Waals interactions at the different torsional strains.

We calculate W_f, the work done by friction under isothermal condition, from the relative torsional displacement of the inner shell and the outer shell from $W_f = W_\tau - \Delta E_s - \Delta E_W$, where W_τ is work done by the external torque, ΔE_s is the strain energy change, and ΔE_W is the change of van der Waals energy due to interlayer interactions. Finite element analysis yields $W_\tau = 258$ eV.ΔE_s is calculated to be 253 ± 4 eV by $\Delta E_s = \pi G (r_o^4 - r_i^4)(\theta_f^2 - \theta_i^2)/4L$, where θ_f, θ_i are the final and initial twist angles, r_o and r_i are the radii of the outer shell and the inner shell, respectively, and L is the length of the tube [22]. The uncertainty of W_τ is estimated by the upper-lower bound method. The standard Lennard-Jones potential is used for the calculation of the total interlayer potential energy $E_{\text{pot}} = 4\varepsilon \sum_{i=1}^{N_i} \sum_{j=1}^{N_o} [(\sigma/r_{ij})^{12} - (\sigma/r_{ij})^6]$, where i donates an atom in the inner shell and j an atom in the outer shell, N_i and N_o are the total number atoms of the inner and outer shells, r_{ij} is the distance between the ith atom and jth atom, and $\varepsilon = 3.622$ meV/atom, and $\sigma = 0.385$ nm are constants (the upper cutoff distance of Lennard-Jones potential is taken as 5 times the C-C bond length) [23]. The change of van der Waals energy from 117° to 147° is 0.37 eV. Thus, the work of friction is $W_f = 4.63 \pm 4$ eV. This yields an average kinetic friction force $f_k = (2.1 \pm 0.9) \times 10^{-9}$ N $[(2.6 \pm 1.0) \times 10^{-15}$ N/atom] obtained from $W_f = \frac{1}{2} f_k \Delta\theta (r_i + r_o)/2$, and $\Delta\theta$ is the relative angular displacement of outer shell to innershell when the paddle is rotated from 117° to 147°. This is 1.2×10^{-15} N/atom larger than the upper-limit value of kinetic friction measured in a telescoping motion in a MWNT [16]. The difference may be due to the following two factors: first, the telescoping motion was measured by a method that prejudicially slides the layers with the least interlayer interaction within a MWNT. Instead, we measure the torsional motion in a randomly selected DWNT. Second, the interaction area never changes in our experiment but it was constantly shrinking in the telescoping motion, which further biases those results to lower values.

The experimental method and the device structure described in this work can also be extended to measure the properties of other types of nanotubes.

The authors wish to thank Professor Jie Liu of Duke University for help in carbon nanotube growth and NSF (NSF-ECCS 0725759) for funding this project.

[1] S. Iijima, Nature (London) **354**, 56 (1991).
[2] S. Iijima and T. Ichihashi, Nature (London) **363**, 603 (1993).
[3] D. S. Bethune, C. H. Kiang, M. S. Devries, G. Gorman, R. Savoy, J. Vazquez, and R. Beyers, Nature (London) **363**, 605 (1993).
[4] M. P. Anantram and F. Leonard, Rep. Prog. Phys. **69**, 507 (2006).
[5] Y. Shibutani and S. Ogata, Model. Simul. Mater. Sci. Eng. **12**, 599 (2004).
[6] J. P. Lu, Phys. Rev. Lett. **79**, 1297 (1997).
[7] L.-C. Qin, J. Mater. Res. **9**, 2450 (1994); A. A. Lucas, V. Bruyninckx, and P. Lambin, Europhys. Lett. **35**, 355 (1996).
[8] L.-C. Qin, Rep. Prog. Phys. **69**, 2761 (2006).
[9] S. J. Papadakis, A. R. Hall, P. A. Williams, L. Vicci, M. R. Falvo, R. Superfine, and S. Washburn, Phys. Rev. Lett. **93**, 146101 (2004).
[10] B. Bourlon, D. C. Glattli, C. Miko, L. Forro, and A. Bachtold, Nano Lett. **4**, 709 (2004).
[11] T. Cohen-Karni, L. Segev, O. Srur-Lavi, S. R. Cohen, and E. Joselevich, Nature Nanotech. **1**, 36 (2006).
[12] J. C. Meyer, M. Paillet, and S. Roth, Science **309**, 1539 (2005).
[13] A. M. Fennimore, T. D. Yuzvinsky, W. Q. Han, M. S. Fuhrer, J. Cumings, and A. Zettl, Nature (London) **424**, 408 (2003).
[14] H. G. Craighead, Science **290**, 1532 (2000).
[15] P. A. Williams, S. J. Papadakis, A. M. Patel, M. R. Falvo, S. Washburn, and R. Superfine, Phys. Rev. Lett. **89**, 255502 (2002).
[16] A. Kis, K. Jensen, S. Aloni, W. Mickelson, and A. Zettl, Phys. Rev. Lett. **97**, 025501 (2006).
[17] J. Cumings and A. Zettl, Science **289**, 602 (2000).
[18] Z. Liu, Q. Zhang, and L.-C. Qin, Appl. Phys. Lett. **86**, 191903 (2005).
[19] Z. Liu and L.-C. Qin, Chem. Phys. Lett. **405**, 265 (2005).

[20] A. R. Hall, L. An, J. Liu, L. Vicci, M. R. Falvo, R. Superfine, and S. Washburn, Phys. Rev. Lett. **96**, 256102 (2006).

[21] G. M. Seed, *Strength of Materials: An Undergraduate Text* (Saxe-Coburg, Edinburgh, UK, 2000).

[22] K. S. Nagapriya, O. Goldbart, I. Kaplan-Ashiri, G. Seifert, R. Tenne, and E. Joselevich, Phys. Rev. Lett. **101**, 195501 (2008).

[23] W. L. Guo, W. Y. Zhong, Y. T. Dai, and S. A. Li, Phys. Rev. B **72**, 075409 (2005).